Vibrational anharmonicity results in decreased thermal conductivity of amorphous HfO_2 at high temperature

Honggang Zhang,[1] Xiaokun Gu,[2] Zheyong Fan,[3] and Hua Bao[1,*]

[1]*University of Michigan–Shanghai Jiao Tong University Joint Institute, Shanghai Jiao Tong University, Shanghai 200240, People's Republic of China*

[2]*Institute of Engineering Thermophysics, School of Mechanical Engineering, Shanghai Jiao Tong University, Shanghai 200240, China*

[3]*College of Physical Science and Technology, Bohai University, Jinzhou 121013, China*

(Received 14 October 2022; revised 4 July 2023; accepted 11 July 2023; published 28 July 2023)

While the high-temperature thermal transport in crystalline materials has been recently carefully addressed, it is much less explored for amorphous materials. Most of the existing studies have focused on the low-/mid-temperature range and have generally found the increasing trend of thermal conductivity with temperature and converging to a constant value, mainly due to the temperature dependence of heat capacity. In this work, we investigate the temperature-dependent thermal conductivity of amorphous HfO_2 with three different methods, including molecular dynamics, the Allen-Feldman theory, and the quasiharmonic Green-Kubo method, with the forces extracted from a machine-learning potential parametrized from first principles. While the Allen-Feldman theory and the quasiharmonic Green-Kubo method show the same temperature dependence trend as the previous expectation even at high temperatures, molecular dynamics simulations show a clear decreasing trend of thermal conductivity at high temperatures. By comparing the results from these approaches, we identify that two anharmonic effects, i.e., thermal expansion and vibrational mode softening, are the mechanisms of the decreased thermal conductivity of amorphous HfO_2 at high temperatures.

DOI: 10.1103/PhysRevB.108.045422

I. INTRODUCTION

Understanding thermal transport in amorphous materials at high temperatures is of great importance for thermal applications involving high-power, high-temperature [1], chemically harsh environments and intense radiation [2]. In the past decade, mature theoretical frameworks and advanced simulation approaches [3–6] have been devoted to understanding the thermal transport of crystalline materials at high temperatures. The anharmonic effects including phonon renormalization [6–8] and higher-order phonon scattering [3,4] have been carefully investigated. In amorphous materials, however, thermal transport properties at high temperatures are much less explored.

Through the past few decades, many studies have been carried out to explore the temperature dependence of thermal conductivity of amorphous materials. Experimental measurements have been conducted for amorphous silicon [9,10], silica [11,12], silicon nitride [13], and amorphous carbon [14] and nearly all show that thermal conductivity increases with temperature. These measurements were almost all conducted at temperatures below 1000 K. It is generally difficult to obtain reliable thermal conductivity data above 1000 K, due to thermal radiation losses [2]. On the other hand, theoretical approaches also show a similar increasing trend of thermal conductivity with temperature. For example, the Allen-Feldman (A-F) theory combined with harmonic lattice dynamics calculations shows that thermal conductivity smoothly increases with temperature until reaching a saturated value [15]. Such a trend is believed to result from a similar temperature dependence of heat capacity. Recent molecular-dynamics (MD)-based simulations combined with quantum correction [16–21] can also lead to a similar trend. Moreover, Simoncelli *et al.* [22] have suggested that the thermal conductivity increases with temperature by an equation derived from the Peierls-Boltzmann transport equation. It seems that a consensus on the increasing trend of the thermal conductivity of amorphous materials has been achieved. However, it is still unclear how thermal conductivity of amorphous materials changes at even higher temperatures. We note that, in a recent MD simulation of amorphous silicon [23], there is a single data point displaying a decreasing trend of thermal conductivity with temperatures beyond 600 K. However, it is unclear whether such a trend is general, and what is the possible mechanism of thermal transport at high temperature, which deserves further in-depth investigation.

In this work, we use the homogeneous nonequilibrium MD (HNEMD) method [24] to calculate the thermal conductivity of amorphous hafnia (a-HfO_2) at high temperatures (up to 2000 K). In order to accurately model the interatomic interactions in a-HfO_2 at large scales, here we adopt the neuroevolution potential (NEP) approach [25], which is one of the most efficient and accurate machine-learning framework for constructing interatomic potentials for complex materials and performing large-scale MD simulations. The HNEMD results show a decreasing trend of thermal conductivity with

*Author to whom correspondence should be addressed: hua.bao@sjtu.edu.cn

temperatures in the high-temperature range, which is different from the results of the A-F theory and the recently proposed quasiharmonic Green-Kubo (QHGK) method [20]. We find that by scaling the vibrational mode frequency and force constants based on a vibrational softening factor and modifying the calculation volume based on the MD results, quantitative agreement can be achieved between the HNEMD and the QHGK methods. The vibrational mode softening and thermal expansion are, therefore, identified as the mechanisms underlying the decreasing thermal conductivity with increasing temperature in a-HfO_2.

The organization of this paper is as follows. In Sec. II, we describe the NEP model we trained for a-HfO_2, the atomic models in the calculations, and the methods used for the thermal transport calculations. In Sec. III, we show the results of the temperature dependence of thermal conductivity in a-HfO_2 and identify the origin of reduced thermal conductivity at high temperatures. Finally, the main findings of this work are summarized in Sec. IV.

II. METHODS

A. The neuroevolution potential

We employ a NEP developed by Fan *et al.* [25] as a machine-learning potential to describe the interatomic interactions in HfO_2. All MD simulations using the NEP are performed with the Graphics Processing Units Molecular Dynamics (GPUMD) package (version 2.9 NEP2) [24]. By comparing the NEP with state-of-the-art machine-learning potentials, it has been shown that the NEP method not only achieves good accuracy, but is also more computationally efficient [24].The NEP-based extensive MD simulations show the effectiveness and accuracy of the NEP approach in determining the thermal transport properties of materials [25], the structural properties of amorphous materials [23], and the mechanical properties of materials [26] in realistic situations. The details of the training process can be found in Refs. [25,27]. The training set for HfO_2 consists of 2056 cells collected from Ref. [28], and the dataset parameters are provided in Table SI of the Supplemental Material [29]. The parameters used for training the NEP are available in Table SII of the Supplemental Material [29]. The trained NEP is tested by comparing the energies and atomic forces predicted by quantum-mechanical density functional theory (DFT) calculations and NEP predictions, which reveals a good agreement between the two calculations, as shown in Fig. 1. We calculate the root-mean-square error (RMSE) of the energy and the force as 3.8 meV/atom and 107 meV/Å, respectively, which show the NEP is comparable to the Gaussian approximation potential (force RMSE is 90 meV/Å) [28] in accuracy. We also validate the NEP described in Sec. S2 of the Supplemental Material [29]. In this work, the NEP is mainly used for calculating the thermal conductivity for comparison and for extracting the second-order and third-order force constants for implementing the A-F theory and QHGK methods.

B. Atomic structure

An atomic structure of a-HfO_2 is obtained with a $3.1 \times 3.1 \times 3.1$ nm^3 supercell of cubic HfO_2 containing 2596 atoms

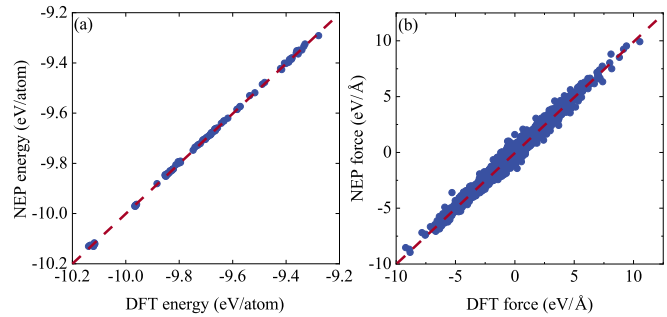

FIG. 1. The comparison of (a) the potential energy and (b) force components between DFT calculations and NEP-based predictions.

undergoing a melt-quench scheme. This domain, which is applied to the subsequent calculations of thermal conductivity using the HNEMD method, the A-F theory, and the QHGK method, is selected after a preliminary size-dependent study (shown in Fig. S2 of the Supplemental Material [29]) on the thermal conductivity. A Nose-Hoover thermostat is used for all melt-quench-anneal process to connect the samples to a heat reservoir. The initial structure is first heated to 4000 K in the isothermal-isobaric ensemble (NPT) for 20 ps. The sample is equilibrated in the canonical ensemble (NVT) for 50 ps at 4000 K and then quenched to 300 K with the quenching rate at 7.4 K/ps in the NPT ensemble within 500 ps. All NPT simulations are performed at zero pressure. For calculating the thermal conductivity at high temperatures, the initial structure is first relaxed at the corresponding temperature in the NPT for 500 ps. The obtained atomic structure is then used to calculate the thermal conductivity. A typical final sample structure is shown in Fig. 2(a). To verify the amorphous structures, we compare the structure factors (See Sec. S4 of the Supplemental Material for calculation details [29]) with the experiment [30] as shown in Fig. 2(b). We can find a very good agreement of our structure factor with that of the experimental x-ray diffraction experiments [30] for a-HfO_2, which confirms the accuracy of the atomic structures.

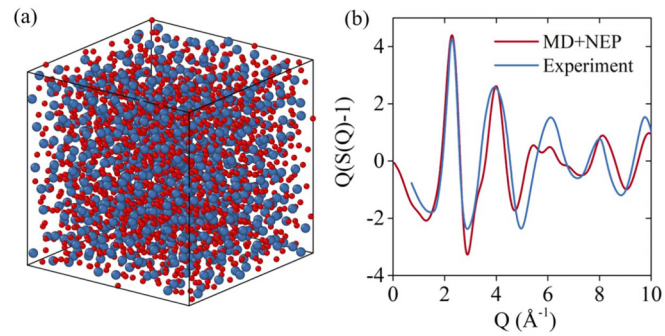

FIG. 2. (a) Structure of a-HfO_2 generated by MD starting from a cubic HfO_2. Blue spheres are for Hf atoms, and red spheres represent O atoms. (b) Comparison of x-ray structure factors for a-HfO_2. The blue curve shows experiment structure factors [30] and the red curve is obtained from MD with the NEP.

C. Thermal transport calculations using the HNEMD method

We first calculate the thermal conductivity from HNEMD methods with GPUMD [24], which is an efficient MD-based method to calculate the thermal conductivity for strongly disordered systems [23]. Note that displacements from molecular dynamics at a desired finite temperature are used to calculate the heat flux, so all orders of anharmonic effect are naturally considered. In this method, the classical spectral thermal conductivity $\kappa(\omega, T)$ as a function of the vibrational frequency ω and the temperature T can be calculated as

$$\kappa(\omega, T) = \frac{2}{VTF_e}\int_{-\infty}^{\infty} e^{i\omega t}K(t)dt, \tag{1}$$

where V is the system volume, F_e is the driving force parameter with the dimension of inverse length, and $K(t)$ is the virial-velocity correlation function (details of the calculations can be found in Ref. [24]). The quantum-corrected thermal conductivity $\kappa_q(\omega, T)$ can be obtained by multiplying the classical one, $\kappa(\omega, T)$, with a ratio between quantum and classical modal heat capacity [17,23],

$$\kappa_q(\omega, T) = \kappa(\omega, T)\frac{x^2e^x}{(e^x-1)^2},\ x = \frac{\hbar\omega}{k_BT}, \tag{2}$$

where $\hbar$ is the reduced Planck constant and k_B denotes the Boltzmann constant.

The thermal conductivity is calculated at zero pressure with the HNEMD method. Periodic boundary conditions are applied in all directions for a-HfO_2. For all the systems, the velocity-Verlet integration scheme with a time step of 1 fs is used. We first equilibrate each system for 2 ns and then apply the external force for 15 ns. The judicious choices of the magnitude of F_e for the systems here are presented in Fig. S3 of the Supplemental Material [29]. In addition, the equilibrium systems at different temperatures are also used for volume and phonon density calculations. In the calculation of thermal conductivity at different temperatures, we randomly perturbed some atoms of the equilibrium system to obtain multiple samples. The average thermal conductivity of all samples is calculated with a proper estimation of the statistical error.

D. The A-F theory and the QHGK method

The thermal conductivity can be computed using the A-F theory [15], which is expressed by

$$k = \frac{1}{V}\sum_i C_i(T)D_i, \tag{3}$$

where V is the volume of the system, $C_i(T)$ is the specific heat of mode i, and

$$C_i = k_B\frac{x^2e^x}{(e^x-1)^2}. \tag{4}$$

Here, we also calculated the effect of temperature on heat capacity using MD simulations and the details are presented in Fig. S4 of the Supplemental Material [29]. We find that at each atom there is still a contribution to the heat capacity by $3k_B$ at relatively low temperatures, while this value is slightly higher when the temperature increases. Therefore, we still use heat capacity theory based on the harmonic approximation to obtain the classical heat capacity, and we use a quantum correction to calculate the quantum heat capacity [Eq. (4)], as has been done in many previous works [15,16,19]. D_i is the diffusivity of mode i. The diffusivities are calculated using

$$D_i = \frac{\pi V^2}{3\hbar^2\omega_i^2}\sum_j^{\neq i}|S_{ij}|^2\delta(\omega_i-\omega_j), \tag{5}$$

where S_{ij} is the heat current operator, which measures the coupling between modes i and j based on the frequency and spatial overlap of eigenvectors,

$$S_{ij} = \frac{\hbar}{2V}v_{ij}(\omega_i+\omega_j), \tag{6}$$

where v_{ij} is the velocity operator and can be computed through

$$v_{ij} = \frac{i}{2\sqrt{\omega_i\omega_j}}\sum_{\alpha,\beta}\sum_{m,l,0}e_l^{i,\alpha}\psi_{lo}^{\beta\alpha}(0)e_o^{j,\beta}(\mathbf{R}_m+\mathbf{R}_{lo}), \tag{7}$$

where $\psi_{lo}^{\beta\alpha}(0)$ is the dynamic matrix and $e_l^{i,\alpha}$ is the phonon eigenvector. $\mathbf{R}_m$ is the position of cell m, and $\mathbf{R}_{lo}$ is the distance between atom l and atom o in a cell.

In Eq. (5), δ is the Dirac delta function, which is approximated by the Lorentzian function,

$$\delta(\omega_i-\omega_j) = \frac{\eta}{\pi[(\omega_i-\omega_j)^2+\eta^2]}, \tag{8}$$

with η being the line-broadening parameter.

In the QHGK method, the mode diffusivities can be expressed by

$$D_i = \frac{1}{3}\sum_j D_{ij} = \frac{1}{3}\sum_j |v_{ij}|^2\tau_{ij}, \tag{9}$$

where τ_{ij} is the generalized lifetime defined as

$$\tau_{ij} = \frac{\Gamma_i+\Gamma_j}{(\Gamma_i+\Gamma_j)^2+(\omega_i-\omega_j)^2} + O(\varepsilon^2), \tag{10}$$

where Γ_i is the linewidth of mode i. The vibrational linewidths can be computed from the classical limit of the Fermi golden rule as

$$\Gamma_i = \frac{\pi\hbar^2}{8\omega_i}\sum_{ml}\frac{|V'''_{jjk}|^2}{\omega_i\omega_j}\Big[\frac{1}{2}(1+n_j+n_k)\delta(n_i-n_j-n_k) + (n_j-n_k)\delta(n_i-n_j-n_k)\Big], \tag{11}$$

where n_i is the Bose-Einstein occupation number of the ith normal mode and $|V'''_{jjk}|$ is the third derivative of the potential energy with respect to the amplitude of the lattice distortion along the lattice normal mode [31].

In the above calculations, the dynamic matrix and the phonon eigenvector are obtained directly in GPUMD based on the lattice dynamics method [32]. The third derivative of the potential energy is obtained using the finite difference approximation methods [33]. In the QHGK simulations, for disordered systems thermal conductivity is not very sensitive to the values of τ_i [20]; therefore, we scale to systems by

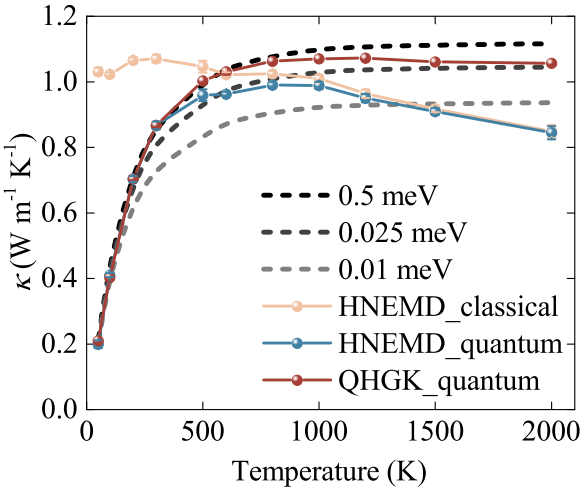

FIG. 3. Thermal conductivity versus temperature for a-HfO_2 using the HNEMD method without or with quantum correction, compared with the A-F theory and the QHGK method. The broadening η used in A-F theory calculations is set equal for each normal mode.

numerically interpolating Γ_i computed for a $4 \times 4 \times 4$ supercell (containing 768 atoms). In order to verify that the initial structure does not significantly affect the thermal conductivity results of the A-F theory and the QHGK method, we calculate the thermal conductivity of three different initial configurations and show that they are similar (shown in Table SIII of the Supplemental Material [29]).

III. RESULTS AND DISCUSSION

The temperature-dependent thermal conductivity is first calculated up to 2000 K with the HNEMD method and is shown in Fig. 3 (denoted as HNEMD_classical). The thermal conductivity almost continuously decreases with temperature, which has also been found in other similar works [19,20]. It is well-known that such an effect is due to the classical nature of MD simulations [34]. The quantum effect must be considered at low temperature [19]. On this basis, the quantum-corrected thermal conductivity is obtained by multiplying the spectral thermal conductivity with a ratio between quantum and classical modal heat capacities [23]. The thermal conductivity after quantum correction is denoted as HNEMD_quantum and is shown in Fig. 3. We can see that the thermal conductivity monotonically increases under 800 K, which is consistent with the previous studies on thermal conductivity of amorphous materials [15,17,19,20,22,35]. However, the thermal conductivity decreases continuously above 800 K. A similar phenomenon has also been observed in recent works for amorphous silicon [20,23].

To identify the origin of reduced thermal conductivity at high temperatures, we also carried out the frequency domain analysis, including the A-F theory and the QHGK method. The A-F theory predicts thermal conductivity based on harmonic approximation. The anharmonic coupling between different modes is considered by introducing an empirical broadening parameter (η). We choose a range of broadening η that includes the broadening η value calculated using the averaged-level spacing method [35]. Here, we use a larger range of linewidths to show that the calculation of the A-F theory depends on the selection of linewidths. Recently, the QHGK method was developed to replace this empirical parameter by a mode-broadening parameter, through weighing diffusive processes between modes with nearly resonant frequencies to consider the anharmonic effect in the process of energy transfer [20]. Both methods consider the mode coupling (i.e., the imaginary part of self-energy), but for the time being we still adopt the zero-temperature mode frequencies as in previous implementations [20]. As shown in Fig. 3, the A-F theory and the QHGK method can both predict thermal conductivity for a-HfO_2. In the low-temperature range, the results for the A-F theory and the QHGK method all agree well with the HNEMD results. As the temperature increases, the impact of η in the A-F theory is more significant. For the QHGK method, even slightly beyond 300 K, the deviation from HNEMD results is non-negligible. At 2000 K, there is a more than 20% difference between HNEMD and QHGK results, which is clearly not due to simulation uncertainty. Therefore, we suspect that some important physics is missing in the current implementation of the QHGK method. Meanwhile, by convention, A-F theory and QHGK methods are based on harmonic approximation, in which the eigenvector and the eigenvalue are calculated by lattice dynamics at 0 K. For crystalline materials, it has been shown that phonon renormalization can play a role at high temperatures [8]. Therefore, we suspect that other anharmonic effects beyond mode coupling, such as vibrational mode frequency change and volume expansion, can play an important role for the temperature-dependent thermal conductivity. These could be the origins of the discrepancies between the HNEMD and QHGK methods at high temperatures.

In particular, atomic diffusion occurs in a-HfO_2, especially at high temperatures [36,37], and it should not be disregarded in the study of thermal conductivity [38]. To assess the influence of diffusion on thermal conductivity in a-HfO_2, we calculated the lifetime of the vibrational mode (the characteristic time for thermal transport) in the QHGK method as shown in Fig. 4(a) below. We can see that the lifetimes of most vibrational modes are of the order of 1 ps. We also calculated the average atomic displacement as a function of time, as shown in Fig. 4(b). We find that the average displacement at this timescale is still below the typical atomic spacing. Based on the fact that the timescale for energy transfer is smaller than diffusion, we suspect that the QHGK method based on the quasistatic atomic position is still reasonable in calculating the thermal conductivity of a-HfO_2. Also, using three different atomic structures yields similar thermal conductivity values in the QHGK method (See Sec. S7 of the Supplemental material for details [29]). Meanwhile, we employed equilibrium molecular dynamics simulations to study the thermal transport in a-HfO_2 at 2000 K (the highest temperature we considered). We find that the contribution from the convective part of the heat current autocorrelation function is essentially 0. The contribution of diffusion in water to thermal conductivity is also very limited (10%) when calculated using the same method [39]. Therefore, we believe that within the temperature range of our study, the contribution of diffusion to thermal conductivity in a-HfO_2 can be neglected, at least in the context of using molecular dynamics simulations. However, further

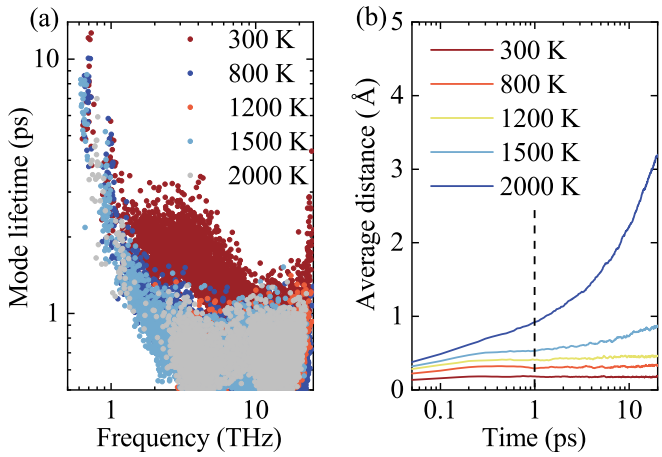

FIG. 4. (a) The vibrational mode lifetimes at different temperatures. (b) The average displacement of atoms at different temperatures. The black dashed line shows the timescale of the vibrational mode lifetime.

research is required to investigate the contribution of diffusion to thermal conductivity under experimental conditions or in other materials.

To confirm our conjectures, we further examine the temperature effect of vibrational mode frequency. For crystalline material, the mode-level frequency shift due to temperature can be obtained with the phonon renormalization. Although similar calculations can, in principle, be carried out with a large cell of amorphous materials, the computational cost is actually formidable [40]. Therefore, we examine the average effect of the mode frequency shift by calculating the vibrational density of states (VDOS) at different temperatures. The VDOS at finite temperature is calculated by the velocity autocorrelation method, while at 0 K the VDOS is calculated using the lattice dynamics method [41] (See Sec. S8 of the Supplemental material for details [29]). As shown in Fig. 5(a), most of the spectra shift to lower frequencies with a rise of temperature, and the peaks at 15 and 22 THz even disappear. The peak at approximately 3 THz slightly red shifts, with a 25% decrease in frequency from 0 to 2000 K. The maximum frequency increases with temperature due to the broadening of the spectral features, and the vibrational states thus appear over a wider range of frequencies. To quantify the overall vibration mode softening at high temperature, we defined a weighted-average frequency at temperature T,

$$\bar{\omega}_T = \frac{\mathrm{VDOS}(\omega, T)\omega d\omega}{\mathrm{VDOS}(\omega, T)d\omega}, \tag{12}$$

where $\mathrm{VDOS}(\omega, T)$ is the vibrational density of states at temperature T. We define a softening factor by $f = \bar{\omega}_T/\bar{\omega}_{\mathrm{LD}}$, where $\bar{\omega}_{\mathrm{LD}}$ is the weighted average frequency calculated from lattice dynamics (0 K). The frequency softening factor is calculated and shown in Fig. 5(b). We can see that f decreases with temperature, indicating that the mode is indeed softened as the temperature increases. On the other hand, the thermal expansion effect leads to an increased simulation cell volume as the temperature increases. To quantify such an effect, we also extract the volume of simulation cell in MD simulation at different temperatures and plot the ratio of volume at finite temperature and volume at 0 K (V/V_0) in Fig. 5(b). We note that the volume of the system increases with the temperature.

In order to consider the vibrational mode softening and thermal expansion in the QHGK method, we modify the input parameters in the QHGK method by scaling the corresponding values. The frequencies are scaled by the softening factor f. The force constant matrix ψ is scaled by a factor of f^2, because from lattice dynamics $\psi \sim \omega^2$ [32]. The volume is replaced by the volume calculated from the MD simulation. In the QHGK method, the mode diffusivities computed by Eq. (9) using the frequency and the force constant matrix with or without modification are compared and the results are shown in Fig. 5(c). The mode diffusivities significantly decrease when using the modified frequency and force constant matrix. According to Eq. (3), the thermal conductivity is predicted to decrease because the mode diffusivity decreases and the volume increases.

The quantum-corrected thermal conductivity of a-HfO_2 using the quantum HNEMD method, compared with the A-F theory and the quantum QHGK method with modified

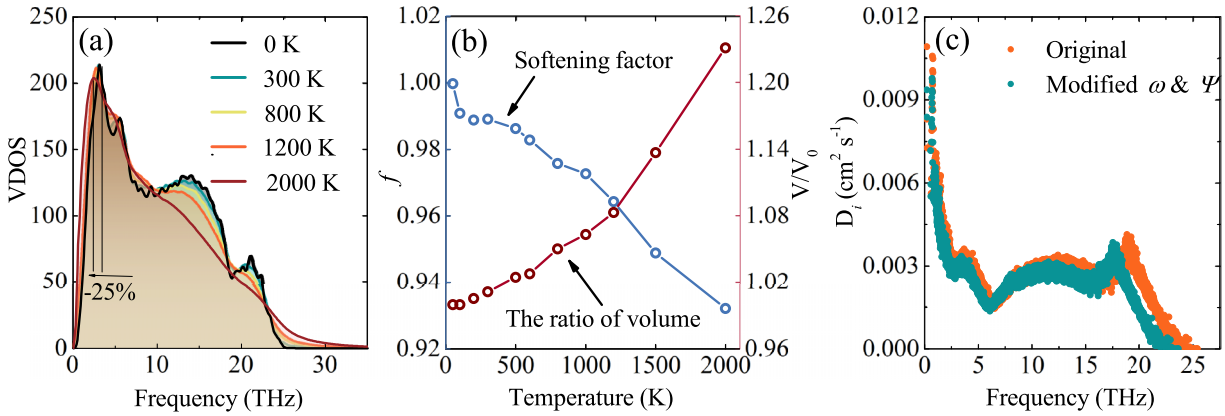

FIG. 5. (a) VDOS of vibrational modes at different temperatures. (b) Frequency softening factor f (left) and the ratio of volume at finite temperature and volume at 0 K (right). (c) Comparison of the diffusivities (D_i) computed using the frequency and the force constant matrix with or without modification.

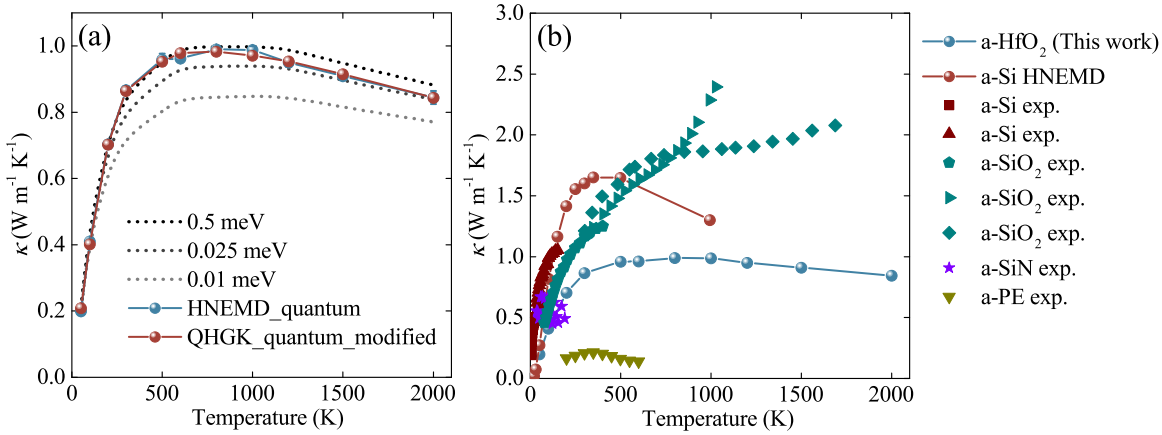

FIG. 6. (a) Quantum-corrected thermal conductivity versus temperature for a-HfO_2 using the quantum HNEMD method, compared with the A-F theory and the quantum QHGK method with modified frequency, force constant, and volume. (b) Thermal conductivity of selected amorphous materials as a function of temperature. Different colors correspond to different amorphous materials: silicon [11,23,42], silica [10,12,43], a-PE [44], and silicon nitride [13].

frequency, force constant, and volume are exhibited in Fig. 6(a). The results calculated by the A-F theory, the quantum QHGK method, and the HNEMD method show a consistent trend of the temperature dependence of thermal conductivity. The thermal conductivity calculated by the HNEMD method and the A-F method is consistent at low temperatures. However, at high temperatures, the thermal conductivity from the A-F method depends on the choice of the broadening parameter. In the simulation of the QHGK method after parameter modification, the obtained thermal conductivities can then quantitatively agree with those from the HNEMD method. Meanwhile, we compare the thermal conductivity spectra calculated by the QHGK and HNEMD methods and find that they are similar to each other (see Fig. S5 of the Supplemental material [29]). Therefore, these results confirm that thermal expansion and vibrational mode softening due to the anharmonic effect lead to the decrease of the thermal conductivity of a-HfO_2 at high temperatures. Moreover, we summarized the reported temperature-dependent thermal conductivities of several common amorphous materials, as shown in Fig. 6(b). We find that the thermal conductivities of a-Si from the HNEMD method and the experimentally measured amorphous polyethylene (a-PE) also show a trend of increasing first and then decreasing. Moreover, we also calculated the thermal conductivity for a-Si, which confirms that the thermal conductivity of a-Si decreases with temperature at temperatures above 600 K (see Fig. S6 of the Supplemental material [29]).The Debye temperatures of a-Si and a-HfO_2 are predicted by $\Theta = hv_m/k_B$ [45] to be 647 and 1104 K, respectively. For a-PE, the Debye temperature is 315 K [46]. The Debye temperatures coincide with the turning point at which the thermal conductivity decreases. However, the thermal conductivity of amorphous silica from experiment seem to increase continuously with temperature. Therefore, a unified mechanism to explain the dependence of thermal conductivity of amorphous materials at high temperatures is still desirable, which should be further studied from the theoretical and experimental perspectives.

IV. CONCLUSION

In conclusion, we explored the temperature-dependent thermal conductivity of a-HfO_2 using the HNEMD method, the A-F theory, and the QHGK method. The results from the HNEMD method reveal a clear decreasing trend of thermal conductivity at high temperatures, while the thermal conductivities calculated by the A-F theory and the QHGK method increase first and then converge to a certain value with increasing temperature. The softening factor defined to quantify the overall difference of frequency with temperature shows that the overall frequency decreases (softening) by 7% from 0 to 2000 K. In addition, apparent thermal expansion is captured by extracting the volumes of simulation cells in MD simulations at different temperatures. We then scale the input parameters in the QHGK method based on the impact of anharmonic effects on the vibration mode frequency, force constants, and volume, and the obtained thermal conductivity can quantitatively agree with those from the HNEMD method. As such, we conclude that two anharmonic effects, i.e., thermal expansion and vibrational mode softening, are the mechanisms of the decreased thermal conductivity predicted by MD methods for a-HfO_2 at high temperatures. This work shows that the previous expectation that thermal conductivity of amorphous materials increases with temperature is not universal. Anharmonic effects can actually reduce the thermal conductivity of some amorphous materials at high temperatures.

ACKNOWLEDGMENTS

This work was supported by the National Natural Science Foundation of China (NSFC) under Grants No. 12104291 and No. 52122606. The computations are carried out on the π 2.0 cluster supported by the Center for High Performance Computing at Shanghai Jiao Tong University. The authors thank Dr. Yanguang Zhou from The Hong Kong University of Science and Technology for useful discussions.

[1] D. R. Clarke and S. R. Phillpot, Thermal barrier coating materials, Mater. Today **8**, 22 (2005).

[2] H. Shanks, P. Maycock, P. Sidles, and G. Danielson, Thermal conductivity of silicon from 300 to 1400 K, Phys. Rev. **130**, 1743 (1963).

[3] T. Feng and X. Ruan, Quantum mechanical prediction of four-phonon scattering rates and reduced thermal conductivity of solids, Phys. Rev. B **93**, 045202 (2016).

[4] T. Feng, L. Lindsay, and X. Ruan, Four-phonon scattering significantly reduces intrinsic thermal conductivity of solids, Phys. Rev. B **96**, 161201(R) (2017).

[5] X. Gu, S. Li, and H. Bao, Thermal conductivity of silicon at elevated temperature: Role of four-phonon scattering and electronic heat conduction, Int. J. Heat Mass Transf. **160**, 120165 (2020).

[6] Y. Xia, K. Pal, J. He, V. Ozoliņš, and C. Wolverton, Particlelike Phonon Propagation Dominates Ultralow Lattice Thermal Conductivity in Crystalline Tl_3VSe_4, Phys. Rev. Lett. **124**, 065901 (2020).

[7] A. Das, B. Chakraborty, S. Piscanec, S. Pisana, A. K. Sood, and A. C. Ferrari, Phonon renormalization in doped bilayer graphene, Phys. Rev. B **79**, 155417 (2009).

[8] X. Qian and R. Yang, Temperature effect on the phonon dispersion stability of zirconium by machine learning driven atomistic simulations, Phys. Rev. B **98**, 224108 (2018).

[9] D. G. Cahill, M. Katiyar, and J. R. Abelson, Thermal conductivity of *a*-Si:H thin films, Phys. Rev. B **50**, 6077 (1994).

[10] D. G. Cahill, H. E. Fischer, T. Klitsner, E. Swartz, and R. Pohl, Thermal conductivity of thin films: Measurements and understanding, J. Vac. Sci. Technol. A **7**, 1259 (1989).

[11] D. G. Cahill, Thermal conductivity measurement from 30 to 750 K: the 3ω method, Rev. Sci. Instrum. **61**, 802 (1990).

[12] H. Kanamori, N. Fujii, and H. Mizutani, Thermal diffusivity measurement of rock-forming minerals from 300 to 1100 K, J. Geophys. Res. **73**, 595 (1968).

[13] A. J. Griffin, Jr., F. Brotzen, and P. Loos, The effective transverse thermal conductivity of amorphous Si_3N_4 thin films, J. Appl. Phys. **76**, 4007 (1994).

[14] A. J. Bullen, K. E. O'Hara, D. G. Cahill, O. Monteiro, and A. Von Keudell, Thermal conductivity of amorphous carbon thin films, J. Appl. Phys. **88**, 6317 (2000).

[15] P. B. Allen and J. L. Feldman, Thermal conductivity of disordered harmonic solids, Phys. Rev. B **48**, 12581 (1993).

[16] K. Sääskilahti, J. Oksanen, J. Tulkki, A. McGaughey, and S. Volz, Vibrational mean free paths and thermal conductivity of amorphous silicon from non-equilibrium molecular dynamics simulations, AIP Adv. **6**, 121904 (2016).

[17] W. Lv and A. Henry, Direct calculation of modal contributions to thermal conductivity via Green–Kubo modal analysis, New J. Phys. **18**, 013028 (2016).

[18] W. Lv and A. Henry, Non-negligible contributions to thermal conductivity from localized modes in amorphous silicon dioxide, Sci. Rep. **6**, 1 (2016).

[19] Y. Zhou, Assessing the quantum effect in classical thermal conductivity of amorphous silicon, J. Appl. Phys. **129**, 235104 (2021).

[20] L. Isaeva, G. Barbalinardo, D. Donadio, and S. Baroni, Modeling heat transport in crystals and glasses from a unified lattice-dynamical approach, Nat. Commun. **10**, 3853 (2019).

[21] H. Zhang, H. Wei, and H. Bao, Thermal transport mechanism of amorphous HfO_2: A molecular dynamics based study, J. Therm. Sci. **31**, 1052 (2022).

[22] M. Simoncelli, N. Marzari, and F. Mauri, Unified theory of thermal transport in crystals and glasses, Nat. Phys. **15**, 809 (2019).

[23] Y. Wang, Z. Fan, P. Qian, M. A. Caro, and T. Ala-Nissila, Quantum-corrected thickness-dependent thermal conductivity in amorphous silicon predicted by machine learning molecular dynamics simulations, Phys. Rev. B **107**, 054303 (2023).

[24] Z. Fan, H. Dong, A. Harju, and T. Ala-Nissila, Homogeneous nonequilibrium molecular dynamics method for heat transport and spectral decomposition with many-body potentials, Phys. Rev. B **99**, 064308 (2019).

[25] Z. Fan, Improving the accuracy of the neuroevolution machine learning potential for multi-component systems, J. Phys.: Condens. Matter **34**, 125902 (2022).

[26] P. Ying, H. Dong, T. Liang, Z. Fan, Z. Zhong, and J. Zhang, Atomistic insights into the mechanical anisotropy and fragility of monolayer fullerene networks using quantum mechanical calculations and machine-learning molecular dynamics simulations, Extreme Mech. Lett. **58**, 101929 (2023).

[27] Z. Fan, Z. Zeng, C. Zhang, Y. Wang, K. Song, H. Dong, Y. Chen, and T. Ala-Nissila, Neuroevolution machine learning potentials: Combining high accuracy and low cost in atomistic simulations and application to heat transport, Phys. Rev. B **104**, 104309 (2021).

[28] G. Sivaraman, A. N. Krishnamoorthy, M. Baur, C. Holm, M. Stan, G. Csányi, C. Benmore, and Á. Vázquez-Mayagoitia, Machine-learned interatomic potentials by active learning: amorphous and liquid hafnium dioxide, npj Comput. Mater. **6**, 104 (2020).

[29] See Supplemental Material at http://link.aps.org/supplemental/10.1103/PhysRevB.108.045422 for (i) the dataset parameters for NEP, (ii) the validation of the NEP, (iii) the results of size effect on the thermal conductivity, (iv) the calculation details for the structure factors, (v) the choices of the magnitude of F_e, (vi) the effect of temperature on heat capacity, (vii) the validation for the A-F theory and the QHGK method, (viii) the calculation details for the vibrational density of states, (ix) the spectral comparison of thermal conductivity, and (x) 17 of the thermal transport calculations for amorphous Si, which include Refs. [23,30,41,47].

[30] G. Sivaraman, L. Gallington, A. N. Krishnamoorthy, M. Stan, G. Csányi, Á. Vázquez-Mayagoitia, and C. J. Benmore, Experimentally Driven Automated Machine-Learned Interatomic Potential for a Refractory Oxide, Phys. Rev. Lett. **126**, 156002 (2021).

[31] J. Fabian and P. B. Allen, Anharmonic Decay of Vibrational States in Amorphous Silicon, Phys. Rev. Lett. **77**, 3839 (1996).

[32] H. Zhao and J. Freund, Lattice-dynamical calculation of phonon scattering at ideal Si–Ge interfaces, J. Appl. Phys. **97**, 024903 (2005).

[33] L. Chaput, A. Togo, I. Tanaka, and G. Hug, Phonon-phonon interactions in transition metals, Phys. Rev. B **84**, 094302 (2011).

[34] J. E. Turney, A. J. H. McGaughey, and C. H. Amon, Assessing the applicability of quantum corrections to classical

thermal conductivity predictions, Phys. Rev. B **79**, 224305 (2009).

[35] J. M. Larkin and A. J. H. McGaughey, Thermal conductivity accumulation in amorphous silica and amorphous silicon, Phys. Rev. B **89**, 144303 (2014).

[36] W. Shen, N. Kumari, G. Gibson, Y. Jeon, D. Henze, S. Silverthorn, C. Bash, and S. Kumar, Effect of annealing on structural changes and oxygen diffusion in amorphous HfO_2 using classical molecular dynamics, J. Appl. Phys. **123**, 085113 (2018).

[37] M. Schie, M. P. Müller, M. Salinga, R. Waser, and R. A. De Souza, Ion migration in crystalline and amorphous HfO_x, J. Chem. Phys. **146**, 094508 (2017).

[38] J. Moon, Examining normal modes as fundamental heat carriers in amorphous solids: the case of amorphous silicon, J. Appl. Phys. **130**, 055101 (2021).

[39] K. Xu, Y. Hao, T. Liang, P. Ying, J. Xu, J. Wu, and Z. Fan, Accurate prediction of heat conductivity of water by a neuroevolution potential, J. Chem. Phys. **158**, 204114 (2023).

[40] N. Bernstein, J. L. Feldman, and M. Fornari, Structural model of amorphous silicon annealed with tight binding, Phys. Rev. B **74**, 205202 (2006).

[41] J. Dickey and A. Paskin, Computer simulation of the lattice dynamics of solids, Phys. Rev. **188**, 1407 (1969).

[42] G. Pompe and E. Hegenbarth, Thermal conductivity of amorphous Si at low temperatures, Phys. Status Solidi B **147**, 103 (1988).

[43] K. L. Wray and T. J. Connolly, Thermal conductivity of clear fused silica at high temperatures, J. Appl. Phys. **30**, 1702 (1959).

[44] T. Zhang and T. Luo, Role of chain morphology and stiffness in thermal conductivity of amorphous polymers, J. Phys. Chem. B **120**, 803 (2016).

[45] P. Debye, Zur theorie der spezifischen wärmen, Ann. Phys. **344**, 789 (1912).

[46] M. Shen, W. N. Hansen, and P. C. Romo, Thermal expansion of the polyethylene unit cell, J. Chem. Phys. **51**, 425 (1969).

[47] A. Togo and I. Tanaka, First principles phonon calculations in materials science, Scr. Mater. **108**, 1 (2015).